Experimental study of a naturally-weathered stiff clay.

EXPERIMENTAL STUDY OF A NATURALLY-WEATHERED STIFF CLAY

Maria Clorinda Mandaglio, Nicola Moraci, Marco Rosone, Camillo Airò Farulla

Maria Clorinda Mandaglio, Nicola Moraci
Department of Civil, Energy, Environment and Materials Engineering (DICEAM), Mediterranean University of Reggio Calabria, Reggio Calabria, Italy

Marco Rosone, Camillo Airò Farulla
Department of Civil, Environmental, Aerospace, and Materials Engineering (DICAM), University of Palermo, Palermo, Italy

Corresponding Author:

Nicola Moraci
Department of Civil, Energy, Environment and Materials Engineering (DICEAM), Mediterranean University of Reggio Calabria, Reggio Calabria, Italy

ABSTRACT: Studying the shear strength of a naturally-weathered clay is important to understand rain-induced slope failures in weathered soils. However, experimental studies on naturally-weathered soils are limited. The paper focuses on the laboratory experimental investigation carried out in order to analyse the shear strength of a naturally-weathered stiff clay that can be found in unsaturated conditions in situ. This has an important practical relevance in the evaluation of the stability conditions of the natural slopes where the clay outcrops. Different experimental techniques of measurement of suction were used in order to obtain the soil water retention curve of the clay over a wide range of suctions. Scanning Electronic Microscope (SEM) observations and results of Mercury Intrusion Porosimetry (MIP) tests are also presented to highlight the considerable fabric arrangement modifications at the microstructural level induced by wetting-drying processes. Moreover, isotropic consolidated drained triaxial compression tests on undisturbed and reconstituted saturated specimens and controlled suction triaxial compression tests on unsaturated undisturbed specimens were carried out. The test results allowed examination of the saturated mechanical behaviour of clay and comparison of the mechanical behaviour of the saturated material with that in unsaturated condition.

Keywords: naturally-weathered clay; unsaturated undisturbed clay, water retention behaviour, shear strength.

1. INTRODUCTION

Landslides are one of the natural disasters that cause major damage worldwide. In the triggering mechanisms of rainfall induced landslides, changes in pore-water pressure within the involved soils play a role of considerable importance. During dry seasons, soil layers near the slope surface are initially unsaturated, and negative pore-water pressure contributes to the shear strength of the soil and hence to slope stability. During wet seasons, rainwater infiltrates into the soil and the negative pore-water pressure may decrease significantly. The wetting and drying cycles controlled by atmospheric changes, result in significant changes in suction that can produce soil degradation especially in marly clays (Cardoso 2007, Alonso et al. 2010). This can contribute to the triggering of the landslides in clay soils. Under such condition, the knowledge of shear strength of soils in saturated and unsaturated states is important to understand the causes of triggering.

In September 2000 in Calabria (Southern Italy), more than 1000 shallow slope failures were triggered by heavy rainfall. The movement often started in slightly concave slopes (zero order basins), frequently at natural or artificial breaks in the slope. The storm of September 2000 was preceded by a long dry period and took place in a season not noted for severe weather events.

The effects of weathering on soil properties and environmental conditions played a key role in the spatial distribution of the triggered instabilities that involved weathered layers on different bedrocks (Mandaglio et al. 2015, 2016).

This work is part of a wide experimental research on the mechanical behaviour of Roccella Clay, a bonded stiff clay that originated from the deposition of a marly clay slurry in a marine environment (Gullà et al. 2005, 2006). In the paper, Scanning Electronic Microscope (SEM) observations and results of Mercury Intrusion Porosimetry (MIP) tests are presented to highlight the considerable fabric arrangement modifications at the microstructural level induced by wetting-drying processes. The key experimental results obtained on saturated and unsaturated undisturbed naturally-weathered specimens of Roccella Clay by isotropic consolidated drained compression load triaxial tests (ICD-CL) and controlled suction triaxial tests are presented and critically discussed. Moreover, in order to obtain the water retention curve of investigated soils, matric and total suction measurements have been carried out using different techniques.

65 The obtained results fall within the framework of the unsaturated experimental testing studies on
66 undisturbed specimens of natural clay which are lacking in the literature (Sheng et al. 2011).
67
68 ## 2. TESTED MATERIAL
69 Roccella Clay is a weak rock deposited in a deep and open marine environment during the Pliocene age. It is
70 an overconsolidated, stiff, marly clay of greyish-white colour. The geological history of the soil is
71 characterized by different processes: the slurries were consolidated during the deposition under the load of
72 the deposited layers, then the deposits were uplifted and subjected to erosion. Consequently, the saline pore
73 water of the marine deposits has been replaced by fresh water along the fissures developed during the uplift.
74 Then, the shallow layers were submitted to several wetting-drying cycles. In situ, the soils are naturally
75 weathered and partially saturated. Block samples were taken from a slope at depths ranging from 0.3 to 1.0
76 m. Table 1 and Figure 1 show, respectively, the average values of the index properties, the main
77 characteristics and the grading envelope of the tested material. The soils can be classified, according to the
78 Unified Soil Classification System (USCS), as high-plasticity clays (CH).
79 The soil mineralogy, analysed by X-ray diffraction (*XRD*), has shown that the main constituents are calcite,
80 quartz, chlorite, kaolinite, muscovite and biotite. The clay minerals are mostly kaolinites and chlorites, as
81 confirmed by the values of plasticity index (27 %) and limit liquid (56.5 %). The carbonate content of the test
82 specimens evaluated by calcimeter analysis varied between 47% and 56%.
83 Some tests were carried out on reconstituted samples prepared adding a quantity of water equal to 1.5 w_L
84 (Burland 1990). The consolidation phase was carried out using a Proctor apparatus modified by inserting
85 perforated plates at the base and at the top to allow the flow of water. The samples were reconstituted as if
86 they were at a depth of about 60 cm (average height of the altered material), placing a weight of 20.5 kg on
87 the porous disc. Cylindrical specimens were then obtained from these samples.
88
89
90 ## 3. MICROSTRUCTURAL ANALYSIS

The hydro-mechanical behaviour of Roccella clay is strongly influenced by the weathering process which enables considerable fabric arrangement modifications at the microstructural level (Gullà et al. 2006). Microstructural analyses were carried out by scanning electronic microscope (SEM) observations using a JEOL JSM – 5600LV microscope.

The undisturbed soil microstructure showed aggregated and flocculated interparticle associations with face-to-face contact (Figure 2). The comparison between SEM microphotographs obtained from spot analyses on undisturbed specimens and those on specimens subjected to different numbers of wetting–drying–freezing–thawing cycles showed that the degradation cycles did not produce mineralogical changes but significant microstructural changes in the soils (Gullà et al. 2006; Mandaglio and Moraci 2008) (Figure 3).

Moreover, mercury intrusion porosimetry (MIP) tests were also carried out. The tests were performed using a porosimeter (Pascal 140–240 series Thermo Scientific Corp.) attaining a maximum intrusion pressure of 200 MPa which corresponds to an entrance pore diameter of approximately 7nm. Macropores were detected at the beginning of the tests in the low pressure unit operating between 0 and 400 kPa. The advancing non-wetting contact angle between mercury and the clay minerals was assumed to be equal to 140° (Romero and Simms 2008). *MIP* tests were carried out on naturally weathered specimens and on specimens that have undergone drying-wetting-drying (DWD). The DWD specimens have been trimmed from a undisturbed sample and then they have been subjected to a drying path in laboratory conditions, corresponding to total suction equal to 110 MPa (T = 20°C and RH ≈ 45%), a wetting path up to 2 MPa and a final intense drying in a heater at 100 °C. However, before *MIP* tests, samples were dehydrated by means of a freezing-drying technique consisting in quick freezing the samples by dipping them in liquid nitrogen (boiling temperature -198°C) and sublimation with vacuum pump at -60°C for 24 h.

Figure 4 shows the results of *MIP* tests in terms of cumulative intruded void ratio (e_{Hg}) and pore size density function ($PSD = -\Delta e_{HG} / \Delta(logD)$) as a function of the entrance pore diameter, D. Collected data analysis confirms that the structure at microscopic level of a naturally weathered clay specimen (e_o = 0.801) presents a single porosity network, where the characteristic pore diameter value corresponds to diameter equal to D = 0.19 μm (Figure 4). The test results also show that intense artificial weathering cycles modify the microstructure of the naturally weathered clay. The cumulated intrusion void ratio of weathered laboratory

specimen (e_i = 0.726) is higher than that of undisturbed naturally weathered specimen (e_i = 0.678) because macropores of equivalent diameter in the order of 10 – 20 μm develop within aggregates. In fact, a slight increase of mean pore diameter (D = 0.21 μm) was observed. The difference ($e_0 - e_i$) between measured and overall intruded void ratio varies in the range between 0.123 (naturally weathered specimen) and 0.060 (DWD laboratory specimen) and is the consequence of non-detected porosity due to the limited capacity of the porosimeter to enter the smallest pores and the entrapped pores.

4. WATER RETENTION PROPERTIES

Soil-water retention curves of undisturbed naturally weathered specimens, in wetting and drying paths, were evaluated using different complementary experimental techniques in order to obtain the soil-water of retention properties in a wide range of suction (0.01 ÷ 110 MPa). In particular, the experimental techniques used were the axis translation technique in a controlled suction oedometer (matric suction tests in the range of s = 0.01 – 0.8 MPa) and indirect measurement techniques of suctions, in the range higher than 2 MPa, by means of WP4-T dewpoint potentiometer device (Decagon Devices Inc.) and by the filter paper method.

Moreover, the results from mercury intrusion porosimetry (MIP) tests have also been used to obtain information on the water retention properties of Roccella clay. In fact, the injection of non-wetting mercury was assumed to be equivalent to the ejection of water from the pores by the non-wetting front advance of air (Romero et al. 1999). The void ratio not intruded by mercury was used to evaluate the degree of saturation corresponding to the imposed equivalent suction. The relation between the pressure of the mercury intrusion, p, and the matric suction, s, for the same pore diameter is expressed as follows:

$$s = -\frac{\sigma_W \cos\theta_W}{\sigma_{HG} \cos\theta_{nw}} p = 0.196\, p \qquad (1)$$

Where σ_w and σ_{HG} are the water and mercury surface tensions, θ_w is the contact angle of the air/water interface (0°), and θ_{nw} is the non-wetting contact angle between the mercury and the soil grain (assumed equal to 140°) (Ferrari et al. 2013).

In the controlled suction oedometer, matric suction was applied by means of the axis translation technique, keeping a constant pore air pressure, u_a = 1000 kPa, and varying the applied pore water pressure, u_w,

144 according to the air overpressure technique (Romero 2001). In order to reduce air diffusion through the high
145 air entry value (HAEV) ceramic disk (nominal air entry value of 1500 kPa), applied pore water pressure at the
146 base of the tested specimens was never reduced below 200 kPa (Airò Farulla and Ferrari 2005). After the
147 reference air pressure translation, tested specimens, with height h = 20 mm and diameter d = 50 mm, were
148 allowed to equalise at suction s_0 = 800 kPa and vertical net stress σ_v = 50 kPa. Then, the specimens were
149 wetted to s = 10 kPa by step of suction at constant vertical net stress and a drying path to s = 800 kPa was
150 accomplished. During the test, volumetric deformations and water content were measured by means of a
151 micrometer, with a resolution of 0.001, and by a burette connected to a water pressure circuit, respectively.
152 The *WP4-T* device quickly measures the water potential using the chilled-mirror dewpoint technique and it
153 allows a constant internal temperature to be maintained since the water potential is influenced by
154 temperature. It measures water potential from 0 to -300 MPa. The cylindrical specimens have height h = 6
155 mm and diameter d = 35 mm, and are placed in a disposable sample cup completely covering the bottom of
156 the cup. Typically, the equalization stages require approximately 5 minutes for each suction increment. The
157 water potential of the specimen can be found by the relationship between the water potential of the
158 specimen (Ψ) in kPa and the vapour pressure of the air, as follows:

159 $$\Psi = \frac{RT}{M} \ln \frac{p}{p_0} \qquad (2)$$

160 where p is the vapour pressure of the air (kPa), p_0 is the saturation vapour pressure at specimen temperature
161 (kPa), R is the gas constant (J/mol·K), T is the Kelvin temperature of the specimen (K) and M is the molecular
162 mass of water (kg/kmol).
163 Suction measurements in the wetting and drying paths were performed. The specimens were dried until
164 equalization at laboratory condition, corresponding to total suction equal to 110 MPa (T = 20°C and RH ≈
165 45%). Then they were wetted in stages by adding drops of distilled water onto the material, stored for 1 day
166 equalization, weighed and the total suction was measured. At the end of the multistage wetting procedure,
167 the specimens were weighed, oven-dried and the water contents back-calculated.
168 Table 2 summarizes the initial properties of two specimens (RCDW1 – RCDW2) subjected to the WP4-T tests
169 and of the specimen subjected to the oedometer test (RCDW3).

In order to validate the results obtained with different techniques, complementary information was gathered through measurements of the total and matric suction using, respectively, non-contact and contact filter paper methods (ASTM D5298-10). These are well known indirect methods (Chandler and Gutierrez 1986; Ridley 1993) based on the water retention properties of a calibrated filter paper (Whatman N. 42). Equilibration time of about 2 weeks is required. After the initial suction measurements, a drying path was applied to the specimen by air-drying under laboratory-controlled conditions for few hours. After, 1-2 days of curing, indispensable to allow the redistribution of the water within the specimen, total and matric suction were measured (Fig. 5). At the end of measurements, the specimen was weighed, oven-dried and the water contents back-calculated.

Figure 5 shows the water retention curves of Roccella Clay obtained by means of the different methods.

Initial conditions of undisturbed specimens, shown in Figure 5 and Table 2, show that undisturbed Roccella Clay may be considered *quasi-saturated* because the degree of saturation is in the range between $S_{r,0}$ = 0.92 - 0.98. Initial matric and total suction measured with filter paper technique were, respectively, in the range s = 1.0 - 1.2 MPa and Ψ = 2.8 - 3.0 MPa. Starting from these experimental data, the osmotic suction has been calculated ($\pi = \Psi - s$) and is equal to about 1.8 MPa. This high value could be the result of high carbonate content partially dissolved in pore water.

Moreover, it can be noticed that the degree of saturation in the main drying water retention curve starts to decrease very quickly from a matric suction value higher than 0.5 MPa, corresponding to 2.3 MPa of total suction. Whereas, in the wetting path, specimen saturates when suction is lower than s = 50 kPa, that is, the water entry value is lower than 50 kPa. The comparison between drying and wetting paths obtained using potentiometer or axis translation techniques shows, without distinction, that the hysteric domain between the main drying and main wetting water retention curves is very tight. At a low degree of saturation (less than 0.25), or rather, at high suction, the influence of the drying-wetting history is found to be negligible because water absorption can be assumed as the dominant mechanism in the retention behaviour.

Points representative of the equalization condition of the specimens subjected to the triaxial tests reported later in the paper are also indicated in Figure 5. As discussed in detail in a subsequent section, the data points

196 depict with a good degree of accuracy the hysteresis domain between the main drying and wetting curves in
197 the range of low suction, that is, a high degree of saturation.
198 Moreover, Figure 5 shows the main drying curve obtained by intruded void ratio values coming from MIP
199 tests. It can be noticed that for suction values higher than 1.5 MPa, the curve is very steep as a result of
200 uniform pore size distribution as shown in Figure 4. The estimated drying water retention curve based on
201 MIP data on the undisturbed specimen, although less smooth, is in good agreement with the curve obtained
202 by the axis-translation technique and the filter paper method. However, for the range of suction lower than
203 s = 0.8 MPa, experimental data from controlled suction oedometer test provide a better interpretation of
204 water retention behaviour in terms of matric suction versus degree of saturation.
205 Then, for matric suction higher than 1.5 MPa, the distance between the water retention curve obtained from
206 *MIP* test and the water retention curve obtained from potentiometer measurements represents the osmotic
207 suction component. It can be noticed that it significantly increases only in the range of matric suction higher
208 than 1.5 MPa, corresponding to total suction equal to 3.3 MPa. In fact, osmotic suction increases as water
209 content decreases, along the main drying path, up to 11.5 MPa for S_r = 0.24, due to the increasing
210 concentration of dissolved calcium carbonate.
211 Figure 6 shows the void ratio as a function of water ratio ($e_w = w\, G_s$) in the drying and wetting paths obtained
212 in the different experimental techniques. It can be noticed that the Roccella clay undergoes a low shrinkage
213 when subjected to increasing suction. The shrinkage limit corresponds to e_w = 0.72, that is w = 26.6%, when
214 total suction is equal to Ψ = 3.8 MPa. If after drying, specimens are subjected to a wetting path, the void ratio
215 increases if compared to the corresponding drying branch. This process is clearly evident from Ψ = 2.9 MPa.
216 However, the swelling behaviour can be easily contained. In fact, during wetting and drying paths carried out
217 in controlled suction oedometer (s = 0.01 – 0.8 MPa) applying vertical net stress σ_v = 50 kPa, the maximum
218 variation of void ratio was equal to Δe = 0.017.
219
220 5. STRESS-STRAIN BEHAVIOUR AND SHEAR STRENGTH
221 In order to discuss weathering effects on the shear strength of Roccella Clay in saturated and unsaturated
222 conditions, a comprehensive experimental programme was carried out. For this purpose, saturated triaxial

223 compression tests and controlled suction triaxial compression tests at constant suction and changing net
224 pressure were performed on undisturbed naturally weathered specimens. Moreover, the results of saturated
225 triaxial compression tests on reconstituted saturated clay specimens are also discussed to quantify the effect
226 of microstructure and weathering processes.
227
228 5.1. EXPERIMENTAL EQUIPMENTS AND PROGRAMME
229 Drained triaxial compression tests on undisturbed and reconstituted saturated specimens were carried out
230 by means of a modified Bishop triaxial cell to evaluate the soil strength envelope in saturated conditions and
231 the effect of microstructure. The shearing stage was carried out at constant displacement rates of about 0.3
232 mm/h. This value has been obtained on the base of the consolidation response to estimate a suitable strain
233 rate for shearing stage. The time required to failure was calculated on the base of time representing
234 theoretical 100% consolidation, t_{100}, obtained graphically from volume change square-root time
235 consolidation curve of triaxial specimens. t_{100} was about 1h and, according to method proposed by Head
236 (1986), the calculated strain rate was about 0.3 mm/h. Table 3 summarizes the initial properties and physical
237 characteristics of the test specimens and the cell pressure applied in the isotropic consolidation stage, σ'_c.
238 The controlled suction triaxial compression tests on undisturbed unsaturated specimens were carried out by
239 means of a servo-controlled automated system for unsaturated soils equipped with a Bishop & Wesley triaxial
240 cell (USP38). The system was designed to test cylindrical specimens with diameter d = 38 mm and height h =
241 76 mm. The application of the stress state occurs by means of an independent system made up of four
242 electro-pneumatic converters for the total vertical stress, cell pressure and the pressures of the two
243 interstitial fluids (u_a and u_w). Vertical stress is measured by means of a load cell, while the values of cell
244 pressure and of interstitial fluid pressure are obtained by three pressure transducers. The axial displacements
245 are measured by an LVDT connected to the acquisition system. The radial deformations are determined by a
246 differential pressure transducer which detects the change in water volume in the glass in which the specimen
247 is immersed. Changes in the water content of the specimen are determined by differential transducer
248 connected to two burettes, one used to fix a reference and the other one to record the water volume expelled
249 or absorbed. The suction is controlled by applying, controlling and measuring, independently, positive values

of pore-air and pore-water pressures (axis translation technique). The required suction value was applied by setting constant pore-air pressure u_a and varying water pressure u_w (table 4) through a high air entry value porous disk (*HAEV* equal to 500 kPa).

The peculiarities of the used USP38 cell are: the reduction in the equalization time during the drying and wetting phases since the circuits which transfer the pressure to the interstitial fluids are connected simultaneously to both the top and bottom of the specimen.

The suction controlled triaxial compression tests were carried out following five different stages: axis translation; equalization; drying (increase of suction at constant cell pressure); isotropic compression at constant suction; displacement-controlled shearing at constant cell pressure and suction. At the end of the axis translation stage, mean net pressure $\underline{p_{net}}$ = 20 kPa and suction s = 20 kPa were applied; they remained at a constant value until the specimen equalized (equalization stage). After, the drying (s = 50, 100 and 150 kPa) and isotropic compression stages (p_{net} = 50, 100 and 150 kPa) were performed to achieve shearing condition, as reported in Table 4. The shearing stage was carried out at displacement rates of about 0.054 mm/h. Some preliminary experimental checks were carried out, following the methodology proposed by Escario and Saez (1987), in order to verify the suitability of this strain rate. The deviatoric stage was halted for 3 days to allow to the dissipation of excess water pressure, if it occurred. Then, the test was re-started at the same rate verifying that the shear strength did not increase.

Table 4 summarises the experimental programme, the initial properties and physical characteristics of the tested specimens of unsaturated triaxial tests.

5.2. SHEAR STRENGTH IN SATURATED CONDITION

Figure 7 illustrates the experimental stress-strain curves obtained from the drained triaxial compression tests for the undisturbed saturated specimens at confining pressures of 50, 100 and 150 kPa, in terms of q/p' versus ε_a and the corresponding curves of ε_{vol} versus ε_a, where $q = \sigma'_1 - \sigma'_3$ is the deviatoric stress, $p' = 1/3 \cdot (\sigma'_1 + \sigma'_2 + \sigma'_3)$ is the mean effectives stress, ε_a is the axial strain and ε_{vol} is the volumetric strain.

The test results showed that both peak shear strength and initial stiffness increase with the confining pressure. The maximum dilatancy was found to follow peak conditions. After peak, the shear strength

277 significantly decreases towards a high displacement value. In all specimens, failure was associated with very
278 well defined shear surfaces separating the specimens into two distinct bodies. Strain-localization occurred;
279 therefore, the stress-strain data for axial strains higher than 5% have not been considered significant.
280 Figure 8 shows the experimental curves obtained from the drained triaxial compression tests performed on
281 the reconstituted saturated specimens at confining pressures of 50, 100 and 150 kPa, in terms of *q/p'* versus
282 axial strain, ε_a, and the corresponding curves of volumetric strains ε_{vol} versus axial strains ε_a. As expected, the
283 *q/p'* ratio at failure is constant for the different specimens, therefore both shear strength and stiffness
284 increase proportionally with the confining pressures. The soil behaviour is hardening and the compressibility
285 increases with increasing of applied cell pressure, σ'_c.
286 The observed differences between the shear strength obtained for undisturbed and reconstituted specimens
287 at the same confining pressure may be due to two factors: void ratio at failure and soil structure. In order to
288 quantify the reduction in the shear strength caused by microstructure, the strength envelopes were
289 normalized by σ_{ve}*, where σ_{ve}* is the equivalent pressure on the intrinsic compression curve corresponding
290 to the void ratio of the natural soil at yielding; it is a measurement of the enhanced resistance to compression
291 due to the natural soil structure (Burland et al. 1996). Figure 9 shows the one-dimensional compression curve
292 of the saturated intact clay, the intrinsic compression line (ICL), and the sedimentation compression line (SCL)
293 in the $I_v - log\sigma_v'$ plane, where I_v is the void index ($I_v = (e - e_{100}^*)/(e_{100}^* - e_{1000}^*)$, where e_{100}^* and e_{1000}^* are the
294 void ratios of the reconstituted clay at $\sigma_{v'}$ = 100 and 1000 kPa, respectively), and $\sigma_{v'}$ is the vertical effective
295 stress (Burland, 1990). The yield stress σ'_{vy} of the intact clay is on the right of the ICL due to soil structure
296 (fabric and bonding).
297 The normalized strength envelopes are shown in Figure 10. The analysis of the strength envelopes normalized
298 with respect to the effective equivalent pressure confirms that Roccella stiff clay is a microstructured soil. In
299 fact, the undisturbed envelope lies above that reconstituted after the normalization.
300
301 5.3. SHEAR STRENGTH IN UNSATURATED CONDITION

In order to define the effect of suction on the shear strength of Roccella clay, the results of unsaturated triaxial tests performed at suctions of 50, 100 and 150 kPa, mean net pressures after isotropic compression $p_{net} = p - u_a$ equal to 50, 100 and 150 kPa (Table 4), were analysed.

In Figure 5, in addition to the complete water retention curve mentioned above, the representative points of equalization have been shown, in terms of degree of saturation as a function of matric suction, at the initial condition of the shearing stage. It is correct to consider that at the end of the equalization stage (p_{net} = 20 kPa, s = 20 kPa), specimens were not completely saturated because they swelled slightly (ε_v = -2.8 ÷ -4.3 %) owing to the increase of water content. The equalization stage was considered complete when specimen water content variations lower than 0.02% per day were measured. The double pore water drainage permitted a reduction in the required time for equalization of a range between 160 and 190 hours. Later, the drying to shearing matric suction (s = 50, 100 and 150 kPa) did not significantly change the degree of saturation (S_r = 0.95 ÷ 1.00) and the void ratio ($\Delta\varepsilon_v$ = 0.8 ÷ 1.2 %). In fact, a maximum variation of about $\Delta S_{r,min}$ = -0.05 was measured in the specimens dried to s = 150 kPa. In this stage, the required time was a function of the difference of suction applied and it was in the range between 50 and 160 hours. The criterion to indicate the end of the phase was the same of the saturation stage. Finally, as a result of change of void ratio ($\Delta\varepsilon_v$ = 0.4 ÷ 2.7 %) corresponding to a low reduction of water content, compression steps to shearing mean net stress, p_{net0}, induced a slight increase in the degree of saturation ($\Delta S_{r,max}$ = 0.02). The consolidation curves in terms of volumetric deformation vs. log time plane were S-Shaped curves and, consequently, the end of this stage was estimated by classical criteria of theory of consolidation. However, after 4-5 days, the variation of volumetric deformation was lower than 0.1% per day.

Then, the values of degree of saturation before the shearing stage were in the range (S_r = 0.96 ÷ 1.00) and equalization points depict the well defined hysteresis retention domain plotted in Fig. 5.

Figures 11-13 show the experimental curves obtained from the controlled suction compression triaxial tests for the undisturbed unsaturated specimens at suctions equal to 50, 100 and 150 kPa at variable net pressures in terms of deviatoric stress, q, versus axial strain, ε_a, and the corresponding curves of volumetric strains ε_{vol} versus ε_a and degree of saturation S_r versus ε_a. It can be seen that both the peak shear strength and the soil

328 stiffness increase with increasing suction and net pressure. After the peak, the shear strength considerably
329 decreases towards a high displacement value. The soil behaviour is dilatant and the dilation increases with
330 increasing suction, s, at the same mean net stress p_{net}. However, dilation decreases with the increase of p_{net}
331 at the same suction, s.
332 Failure was associated with very well defined shear surfaces separating the specimens into two distinct
333 bodies (Figure 14). Strain-localization occurred, therefore the experimental data for strains higher than 8%
334 have not been considered significant.
335 The degree of saturation increased slightly during the shearing stage at s = 50 kPa until complete saturation
336 was reached while, in general, it was fairly constant during the shearing stage at s = 100 and 150 kPa. A
337 different evolution of the degree of saturation was observed during tests at s = 150 kPa, where the applied
338 confining pressure markedly affects the unsaturated behaviour. In fact, the specimen sheared at p_{net} = 150
339 and s = 150 kPa exhibited a slight increase in the degree of saturation because of the more compressive
340 behaviour at constant water content after the peak. On the other hand, the specimen sheared at p_{net} = 50
341 and s = 150 kPa exhibited a slight decrease in the degree of saturation because of the more dilatant behaviour
342 at constant water content after the peak.
343 Figure 15 shows the shear strength envelope and the stress paths at different values of suction, s, (0, 50, 100
344 and 150 kPa) in the plane q - p_{net}. According to the collected data, the shear strength of the undisturbed
345 Roccella clay can be characterized by a shear strength angle φ', which as a first approximation can be
346 considered constant, for both saturated and unsaturated specimens in the range to 30 - 33°, and by an
347 intercept cohesion c, varying in the range 113 - 214 kPa, which depends on applied suction.
348 The increase in strength due to the suction of naturally weathered Roccella clay is highly significant
349 considering that the shear strength of reconstituted clay is characterised by null intercept cohesion and shear
350 strength angle equal to φ' = 30°.
351
352 ## 6. DISCUSSION
353 Regarding to the interpreting and modelling experimental data related to the shear strength of unsaturated
354 soils, there is wide consensus for using an effective stress approach. In fact, among the advantages of this

355 approach, it is worth mentioning the smooth transition from saturated to unsaturated conditions and the
356 possibility to evaluate shear strength of an unsaturated soil by using the parameters that characterize its
357 behaviour when it is in a saturated state (Jommi 2000, Laloui and Nuth 2009; Alonso et al. 2010). Thus, in
358 order to consider appropriately the effects of suction on the shear strength of unsaturated Roccella clay, the
359 effective stress definition reported by Tarantino and Tombolato (2005) and Rosone et al. (2016) can be used,
360 as follows:

361 $$\sigma'_{ij} = \sigma_{ij} - u_a \delta_{ij} + \frac{e_w - e_m}{e - e_m}\left(u_a - u_w\right)\cdot \delta_{ij} \qquad (4)$$

362 where e is the void ratio, e_w is the water ratio ($e_w = G_s\, w$) and e_m is the microstructural void ratio. In the
363 equation 4, the Bishop's effective stress parameter (Bishop, 1959) has been defined as $\chi = \frac{e_w - e_m}{e - e_m} = S_{rM}$,
364 that is the macropore degree of saturation. Therefore, a single effective stress shear strength criterion can
365 be defined, as follows:

366 $$q = q_c + p'\cdot M = q_c + \left(p_{net} + s\cdot S_{rM}\right)\cdot M \qquad (5)$$

367 $$q = q_c + \left(p_{net} + s\frac{e_w - e_m}{e - e_m}\right)\cdot M \qquad (6)$$

368 where q_c and M are, respectively, the intercept and the slope of the saturated envelope on the plane *(q, p')*
369 and p_{net} is the mean net stress equal to $p_{net} = ((\sigma_1 + \sigma_2 + \sigma_3) /3) - u_a$.
370 Although in this research some microstructure investigations were carried out with the aim to provide a
371 comprehensive examination about the effect of weathering on microstructure, the determination of the
372 evolution of microstructural void ratio e_m with suction (or water ratio), as suggested by Rosone et al. (2016),
373 requires a more elaborate testing programme.
374 Points representative of peak and critical state condition of the triaxial compression tests on unsaturated
375 clay specimens are plotted in Fig. 16, by representing measured deviatoric stress q values versus mean
376 effective stress p' values, calculated according to the definition:

377 $$p' = p_{net} + s\frac{e_w - e_m}{e - e_m}. \qquad (7)$$

Then, the microstructural void ratio e_m of naturally-weathered clay was obtained as a best fit parameter considering the uniqueness of the failure envelope for both saturated and unsaturated specimens, and it was assumed as invariant in the range of explored suction. Besides, Rosone et al. (2016) have shown that this assumption can be satisfactorily applied to clays with low activity, such as the undisturbed Roccella Clay (I_a = 0.5). As shown in Figure 16, microstructural void ratio e_m equal to 0.70 was obtained and a good accuracy fitting with saturated envelope is shown (R^2 = 0.936). It is worth to highlight that the microstructural void ratio e_m is very close to the water ratio e_w = 0.72 corresponding to the shrinkage limit. Indeed, stress points representing the critical state condition of saturated and unsaturated specimens (grey points in Figure 16) depict, with fair accuracy (R^2 = 0.786), the reconstituted clay envelope. At failure, the strain-localization along a well-defined shear surface affects the overall behaviour of the clay. In fact, in correspondence to the surface, the clay is remoulded by accumulation of deformation and it takes on approximately the same resistance as a reconstituted clay. However, the drop in resistance is more accentuated in unsaturated specimens subjected to swelling during saturation and later drying before the shear stage in controlled suction triaxial compression tests. Besides, Gullà et al. (2006) showed as the wetting and drying path cycles disturbed the natural soil structure, producing changes in fabric and bonding (Figure 3) and the shear strength values of the more weathered specimens approached the values obtained for the reconstituted specimens.

7. CONCLUSION

In the paper, the results of an experimental programme to evaluate the shear strength of a naturally-weathered stiff clay under saturated and unsaturated conditions have been described. Emphasis has been given to the influence of the soil structure on the mechanical response of the natural clay by comparing test results obtained on natural as well as reconstituted materials.

Experimental results showed a softening behaviour in the stress - strain plane on saturated undisturbed naturally weathered specimens while a hardening behaviour and constrained volumetric behaviour on saturated reconstituted specimens. Comparison of peak failure envelopes of the undisturbed and reconstituted specimens in the normalized plane showed the influence of the microstructure, highlighted by the fact that the two envelopes do not coincide even after the normalization by the equivalent pressure.

405 Moreover, *MIP* analysis showed a microstructure, characterized by unimodal pore distribution, typical of
406 reconstituted clay, not yet made stable by the effects of weathering induced by cycles of wetting and drying.
407 Indeed, the development of voids within aggregates and the slight increase of mean pore diameter after
408 intense wetting and drying processes highlighted that naturally weathered Roccella Clay still suffered the
409 consequences of intense weathering processes. Weathering disturbs the natural soil structure, producing
410 changes in fabric and bonding, and induced a degradation of undisturbed clay.

411 Analysis of retention properties of naturally weathering clay underlined the strict relationship between
412 the degree of saturation and suction. Once the air entry value, equal to s = 0.5 MPa, has been exceeded the
413 degree of saturation decreased very quickly to the residual value. Indeed, hysteretic domain between main
414 drying and main wetting water retention curves is very small.

415 Data obtained by suction controlled triaxial compression tests allowed to define the stress-strain
416 behaviour of unsaturated Roccella clay. Both the peak shear strength and the soil stiffness increase with the
417 increase of suction, while the dilatant trend at constant suction decreases with the increase of the mean net
418 stress.

419 The stress-strain curves for the undisturbed unsaturated specimens showed that the behaviour is always
420 softening and the volumetric behaviour is dilatant in function of applied suction and mean net stress.

421 The failure envelope according to a single effective stress shear strength criterion has been defined in
422 order to assess the influence of suction on unsaturated conditions. The uniqueness of shear strength
423 envelope in saturated and unsaturated conditions has been highlighted and it showed that the shear strength
424 envelope at critical state of naturally weathered Roccella clay corresponds to the reconstituted clay envelope.

425 REFERENCES

426 Airò Farulla C. and Ferrari A. (2005). Controlled suction oedometric tests: analysis of some experimental
427 aspects. Proc. Int. Symp. on advanced experimental unsaturated soils mechanics, Experus 2005, Trento, Italy,
428 27-29 June, pp. 43-48, ISBN 0415383374.

429 Alonso E.E, Pereira J, Vaunat J and Olivella S. (2010). A microstructurally based effective stress for
430 unsaturated soils. Geotechnique 60: 913–925.

431 ASTM D5298-10, Standard Test Method for Measurement of Soil Potential (Suction) Using Filter Paper, ASTM
432 International, West Conshohocken, PA, 2010.

433 Bishop A.W. (1959). The principle of effective stress. Teknisk Ukeblad 106(39), 859-863.

434 Burland J.B. (1990). On the compressibility and shear strength of natural clays. Geotechnique, 40(3): 329–
435 378.

436 Burland J.B., Rampello S., Georgiannou V.N. and Calabresi G. (1996). A laboratory study of the strength of
437 four stiff clays. Geotechnique 46 (3), 491-514.

438 Cardoso R. (2007). Degradation of compacted Marls. A micromechanical investigation. XVIII European Young
439 Geotechnical Engineers' Conference, Ancona, Italy.

440 Chandler R. J. and Gutierrez C. I. (1986). The filter paper method of suction measurement. Geotechnique 36,
441 No. 2,265-268.

442 Escario V. and Saez J (1987). Shear strength of partly saturated soils versus suction. Proc. Of International
443 Conference on Expansive Soils, 6, New Delhi, v.2, 141-143

444 Ferrari A., Favero V., and Laloui L. (2013). Experimental analysis of the retention behavior of shales. 47th US
445 Rock Mechanics / Geomechanics Symposium 2013; San Francisco, CA; United States; 23 June 2013. Volume
446 1, 2013, Pages 653-657

447 Gullà G., Mandaglio M.C. and Moraci N. (2005). Influence of degradation cycles on the mechanical
448 characteristics of natural clays. Proceedings of 16th International Conference on Soil Mechanics and
449 Geotechnical Engineering, Osaka (Japan), 12-16 September 2005: 2521-2524.

450 Gullà G., Mandaglio M.C. and Moraci N. (2006). Effect of weathering on the compressibility and shear
451 strength of a natural clay. Canadian Geotechnical Journal 43: 618-625.

452 Head, K. H. (1986). Manual of Soil Laboratory Testing, Vol. 3, Pentech Press Limited, London, Great Britain,
453 p.937.

454 Jommi C. (2000). Remarks on the constitutive modelling of unsaturated soils. In: Tarantino A, Mancuso C
455 (eds) Experimental evidence and theoretical approaches in unsaturated soils. Balkema, Rotterdam, pp 139–
456 153

457 Laloui L. and Nuth M (2009). On the use of the generalised effective stress in the constitutive modelling of
458 unsaturated soils. Comput. Geotech. 36(1–2): 20–23.

459 Leroueil S. (2001). Natural slope and cuts: movement and failure mechanisms. Geotechnique 51, N°3, 197-
460 243.

461 Mandaglio M.C. and Moraci N. (2008). Changes in natural clay microstructure due to laboratory weathering.
462 Environmental Semeiotics journal ISSN: 1971-3460. Interdisciplinary approaches for environment and
463 territory safety. 1(2), 236-246

Mandaglio M.C., Moraci N., Gioffrè D. and Pitasi A. (2015). Susceptibility analysis of rapid flowslides in Southern Italy. International Symposium on Geohazards and Geomechanics 10-11 September, 2015, University of Warwick, Coventry, U.K.

Mandaglio M.C., Moraci N., Gioffrè D. and Pitasi A. (2016). A procedure to evaluate the susceptibility of rapid flowslides in Southern Italy. Landslides and Engineered Slopes. Experience, Theory and Practice: Proceedings of the 12th International Symposium on Landslides (Napoli, Italy, 12-19 June 2016), Vol. 3, pp. 1339-1344, ISBN 978-1-138-02988-0 - DOI: 10.1201/b21520-163

Ridley A. M. (1993). The measurement of soil moisture suction. PhD thesis, University of London.

Romero E. (2001). Controlled suction techniques. 4° Simposio Brasileiro de Solos Nao Saturados. W.Y.Y. Gehling & F. Schnaid (eds), Porto Alegre, Brasil, pp. 535-542.

Romero E. and Simms P (2008). Microstructure investigation in unsaturated soils: a review with special attention to contribution of mercury intrusion porosimetry and environmental scanning electron microscopy. Geotech Geol Eng 26:705–727

Romero E., Gens A. and Lloret A. (1999). Water permeability, water retention and microstructure of unsaturated compacted Boom clay. Engineering Geology, Volume 54, Issue 1-2, September 1999, Pages 117-127

Rosone M., Airò Farulla C. and Ferrari A. (2016). Shear strength of a compacted scaly clay in variable saturation conditions. Acta Geotechnica 11(1):37-50.

Sheng D., Zhou A. and Fredlund D. G. (2011). Shear Strength Criteria for Unsaturated Soils. Geotech. Geol. Eng. 29:145–159

Tarantino A. and Tombolato S. (2005). Coupling of hydraulic and mechanical behaviour in unsaturated compacted clay. Geotechnique 55(4):307–317

Table 1. Mean index properties and physical characteristics of the tested material

w_L (%)	w_P (%)	PI (%)	G_s	γ_d (kN/m^3)	γ (kN/m^3)	e
56.5	29.5	27	2.73	12.44	16.80	1.14

Table 2. Drying/wetting tests

Test	G_S	H (mm)	D (mm)	w_0 (%)	e_0	$S_{r,0}$ (%)	Wetting/drying cycle	Specimen
RCDW1	2.71	5.23	35.0	27.8	0.79	96.9	3÷110 MPa (WP4-T)	undisturbed
RCDW2	2.71	5.23	35.0	27.8	0.77	97.9	3÷110 MPa (WP4-T)	undisturbed
RCDW3	2.71	20.0	50.0	27.6	0.81	91.8	0.01÷0.8 MPa (oedometer)	undisturbed

Table 3. Saturated triaxial tests

Test	G_S	w_0 (%)	e_0	$S_{r,0}$ (%)	σ'_c (kPa)	Specimen
RCU1	2.71	27.5	0.76	97.4	50	undisturbed
RCU2	2.70	27.2	0.82	89.8	100	undisturbed
RCU3	2.71	28.1	0.78	98.2	150	undisturbed
RCR1	2.72	40.6	1.11	99.6	50	reconstituted
RCR2	2.71	39.6	1.07	99.9	100	reconstituted
RCR3	2.71	40.5	1.1	99.9	150	reconstituted

Table 4. Unsaturated triaxial tests

Test	G_S	w_0 (%)	e_0	$S_{r,0}$ (%)	u_a (kPa)	u_w (kPa)	$s=u_a-u_w$ (kPa)	p_{net} (kPa)	Specimen
RCUN1	2.71	29.3	0.83	95.6	250	200	50	50	undisturbed
RCUN2	2.72	28.0	0.79	96.1	250	200	50	100	undisturbed
RCUN3	2.71	27.6	0.79	95.1	250	200	50	150	undisturbed
RCUN4	2.71	27.3	0.82	90.3	250	150	100	50	undisturbed
RCUN5	2.71	28.9	0.83	94.8	250	150	100	100	undisturbed
RCUN6	2.71	27.8	0.81	92.8	250	150	100	150	undisturbed
RCUN7	2.71	25.9	0.74	95.3	250	100	150	50	undisturbed
RCUN8	2.71	27.0	0.84	86.8	250	100	150	100	undisturbed
RCUN9	2.71	26.9	0.79	92.6	250	100	150	150	undisturbed

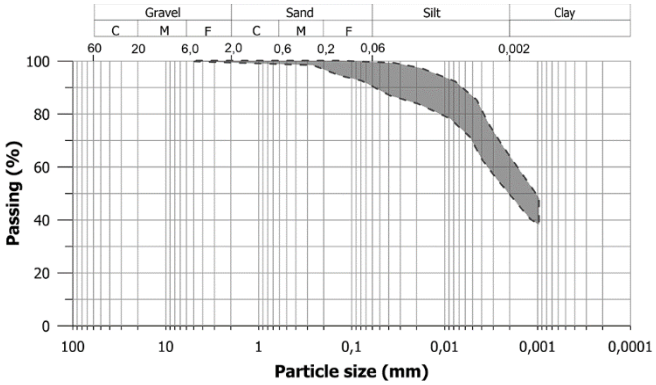

Figure 1 - Grading envelope of tested soils (modified from Gullà et al., 2006).

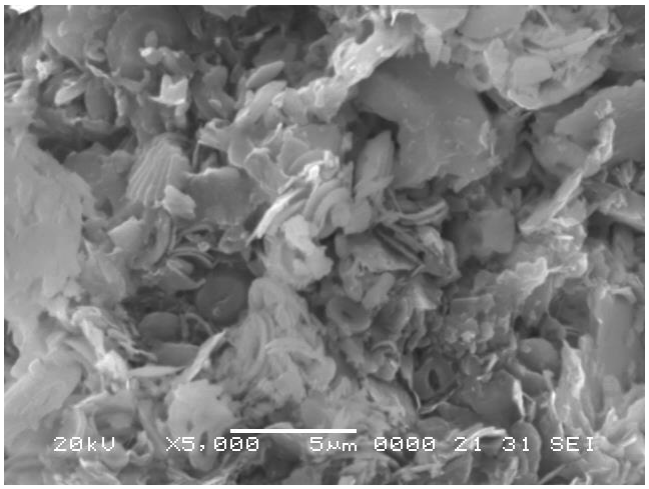

Figure 2 – SEM observation of the clay (5000x) (Gullà et al., 2006).

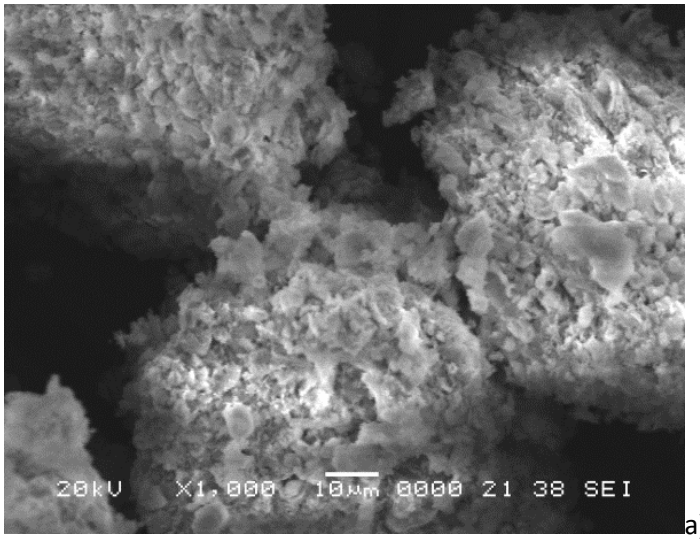

a)

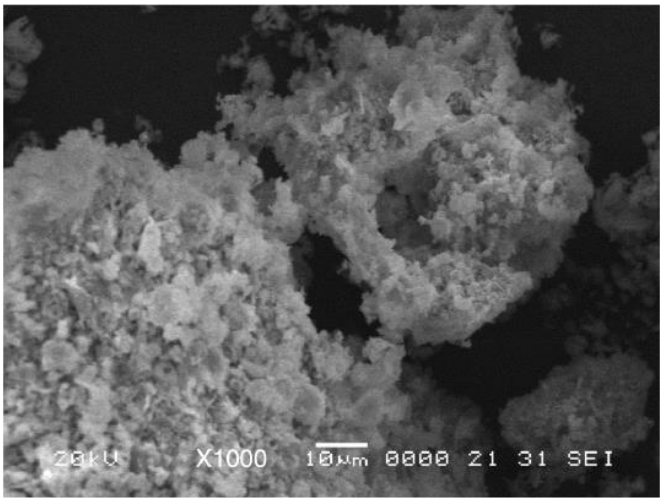

b)

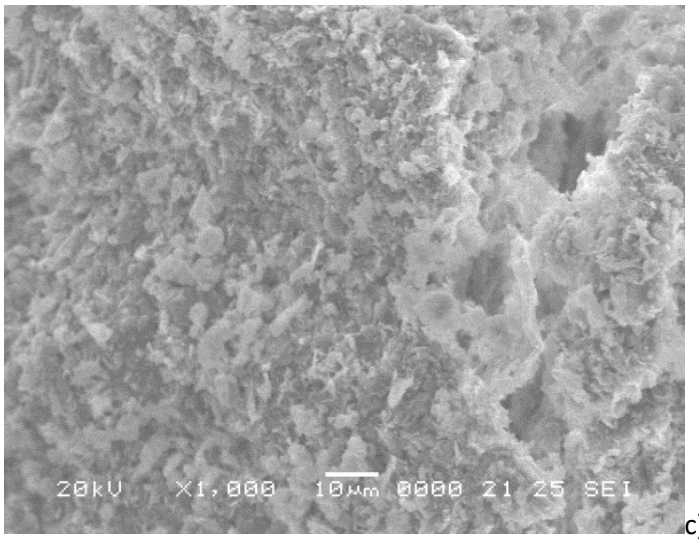

c)

Figure 3 – SEM observations (1000x) of the undisturbed (a), low weathered (b) and high weathered clay (c) (modified from Gullà et al., 2006).

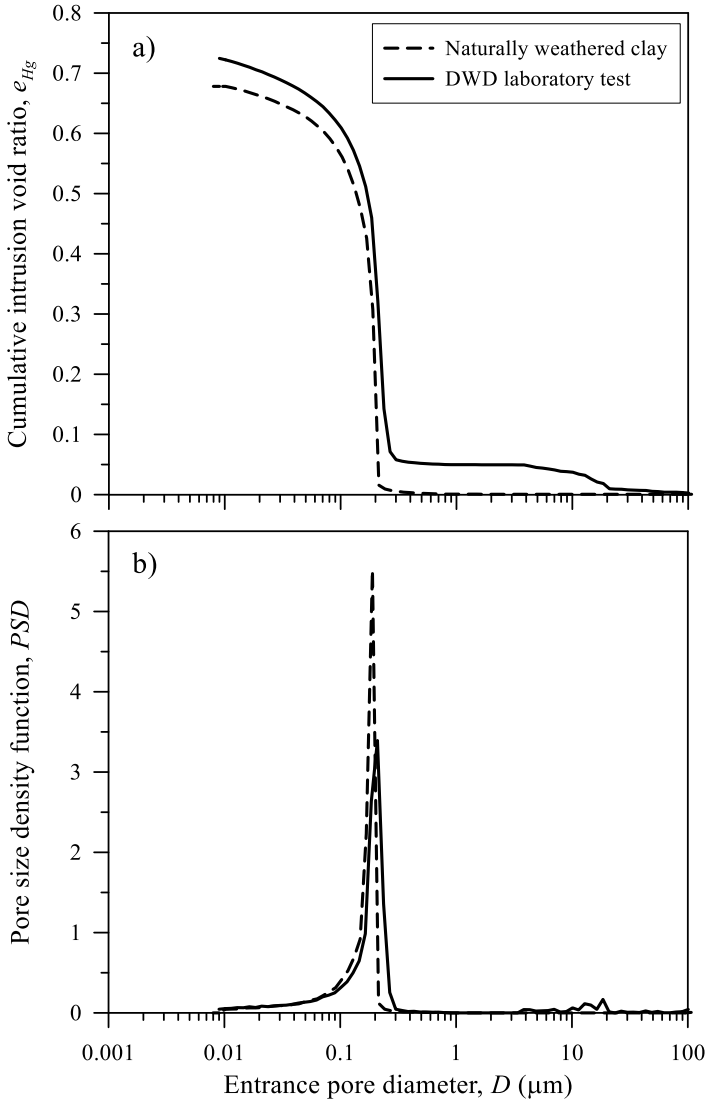

Figure 4 – MIP tests results on undisturbed clay and after Drying-Wetting-Drying cycles (DWD).

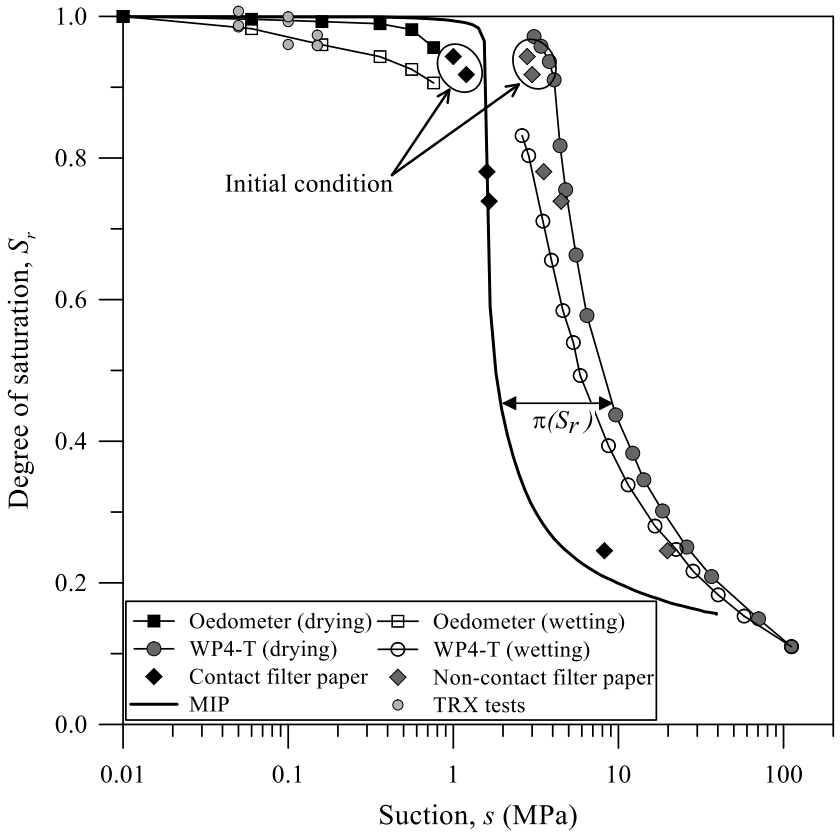

Figure 5 – Water retention curves of naturally weathered Roccella clay.

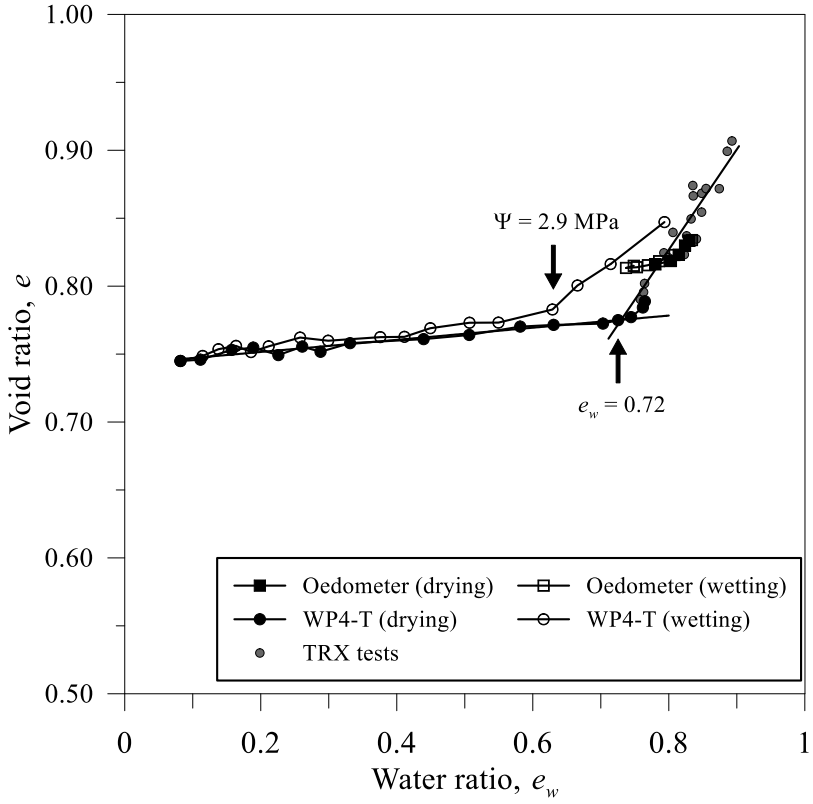

Figure 6 – Drying and wetting paths on the plane (e_w,e).

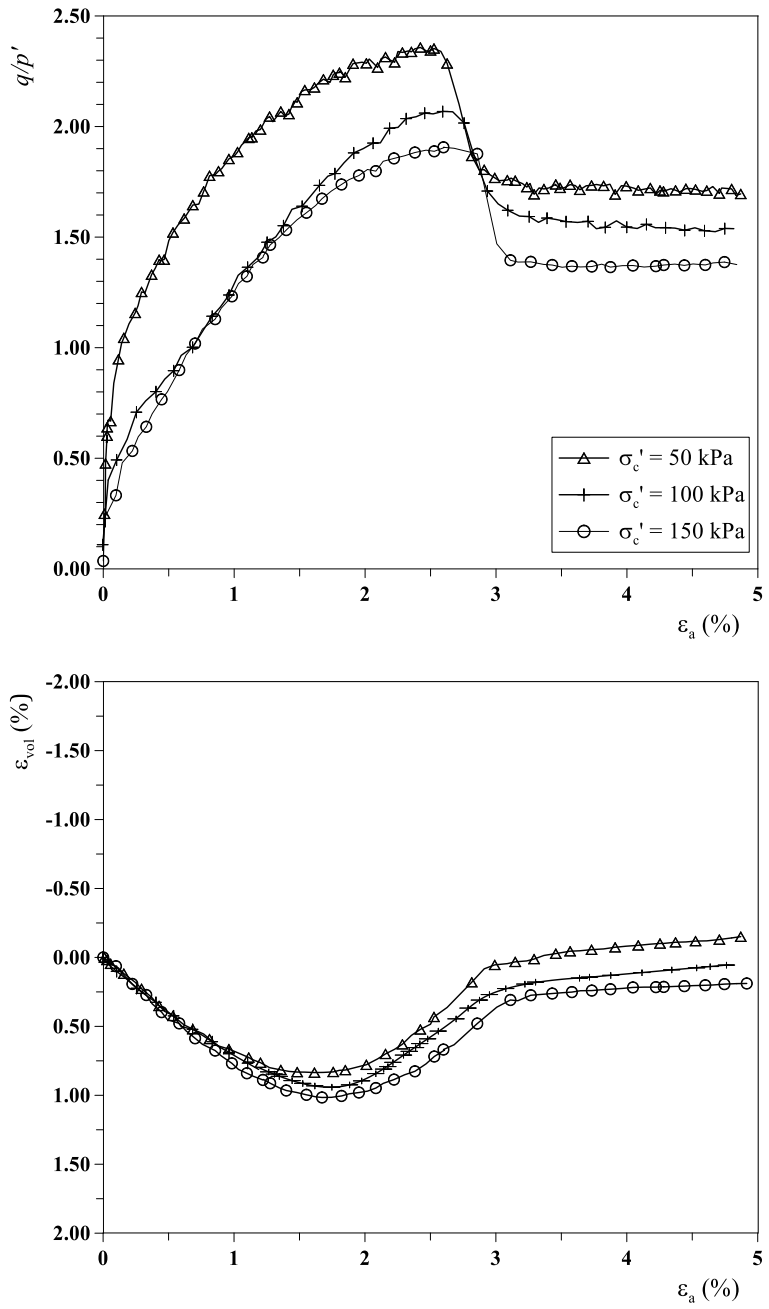

Figure 7 – Results of triaxial compression tests on undisturbed naturally weathered clay.

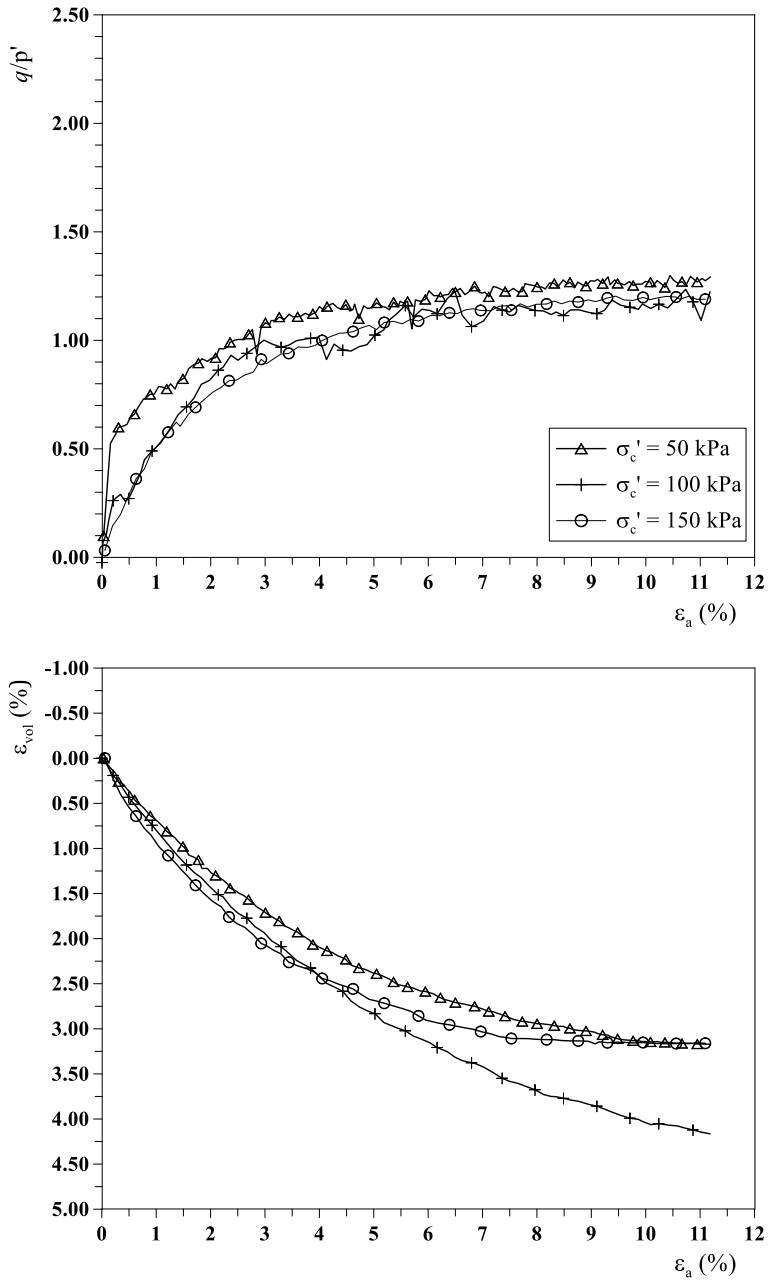

Figure 8 - Results of triaxial compression tests on reconstitued clay.

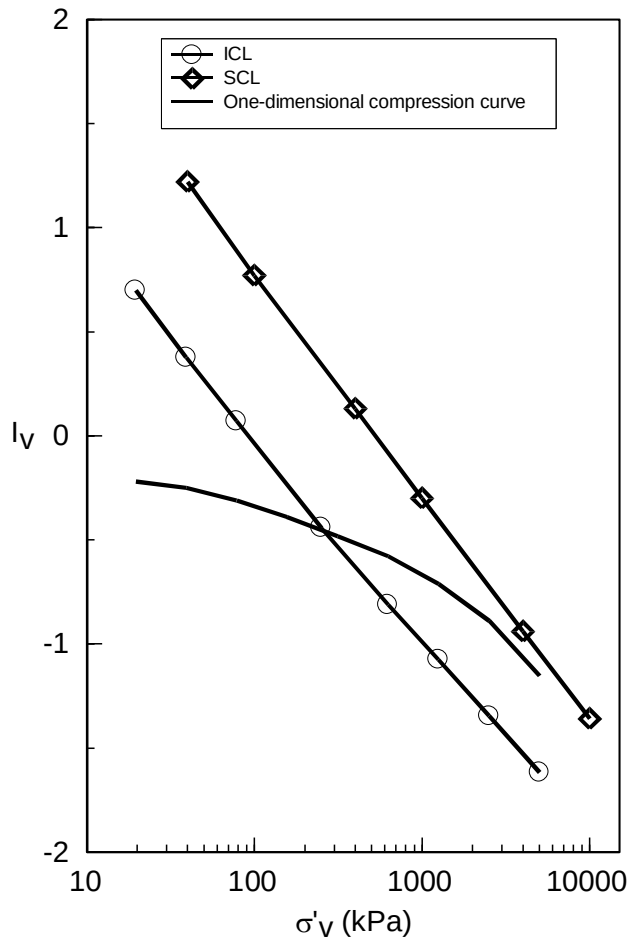

Figure 9 - One-dimensional compression curve, intrinsic compression line (ICL), and sedimentation compression line (SCL) (Gullà et al., 2006).

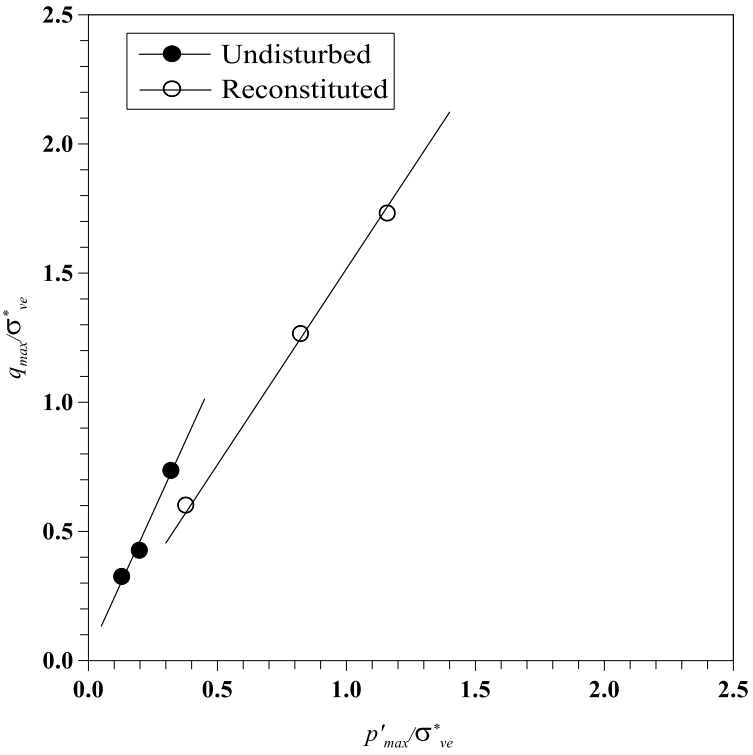

Figure 10 – Normalized shear strength envelopes for undisturbed and reconstituted saturated specimens.

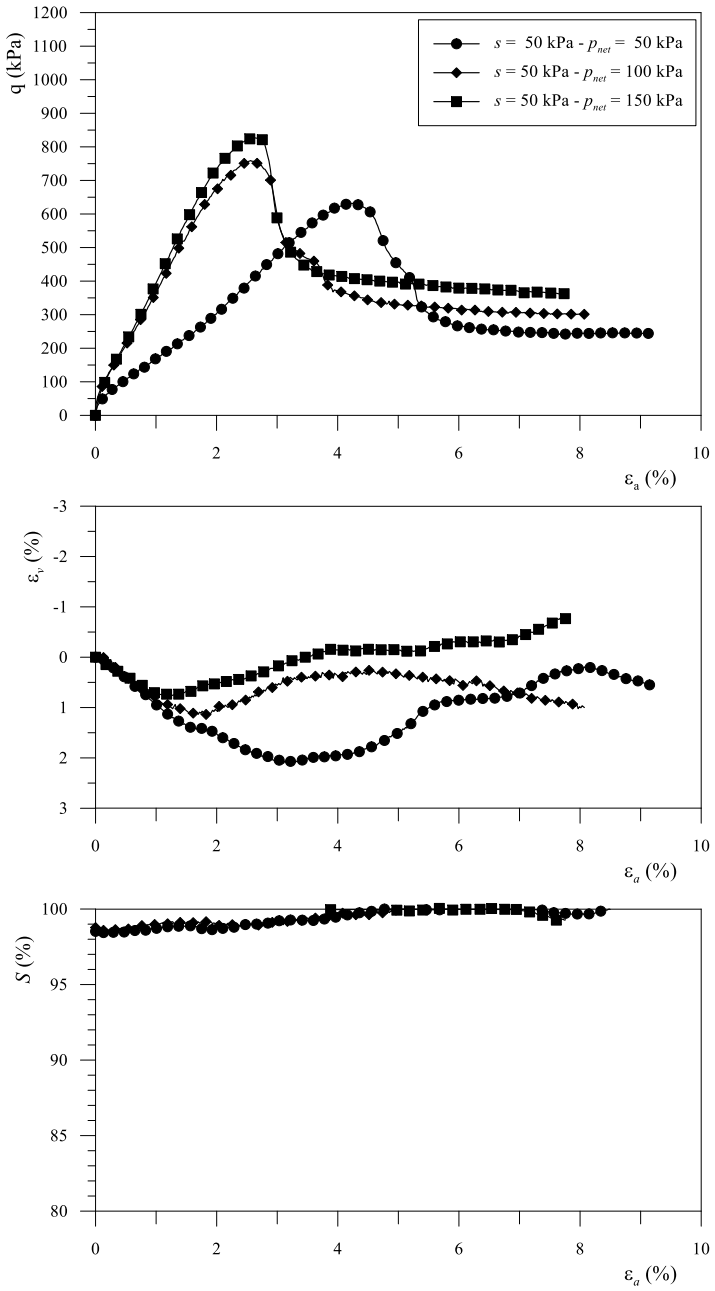

Figure 11 - Results of triaxial compression tests at *s* = 50 kPa.

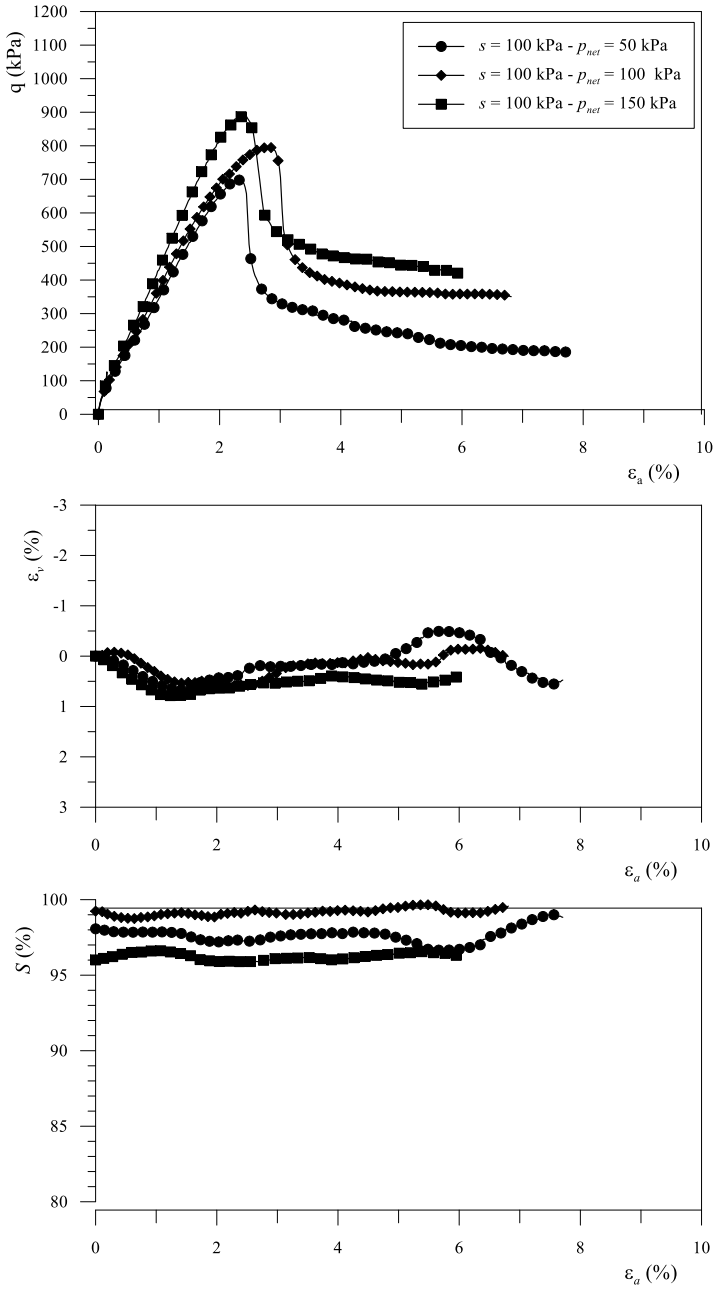

Figure 12 - Results of triaxial compression tests at *s* = 100 kPa.

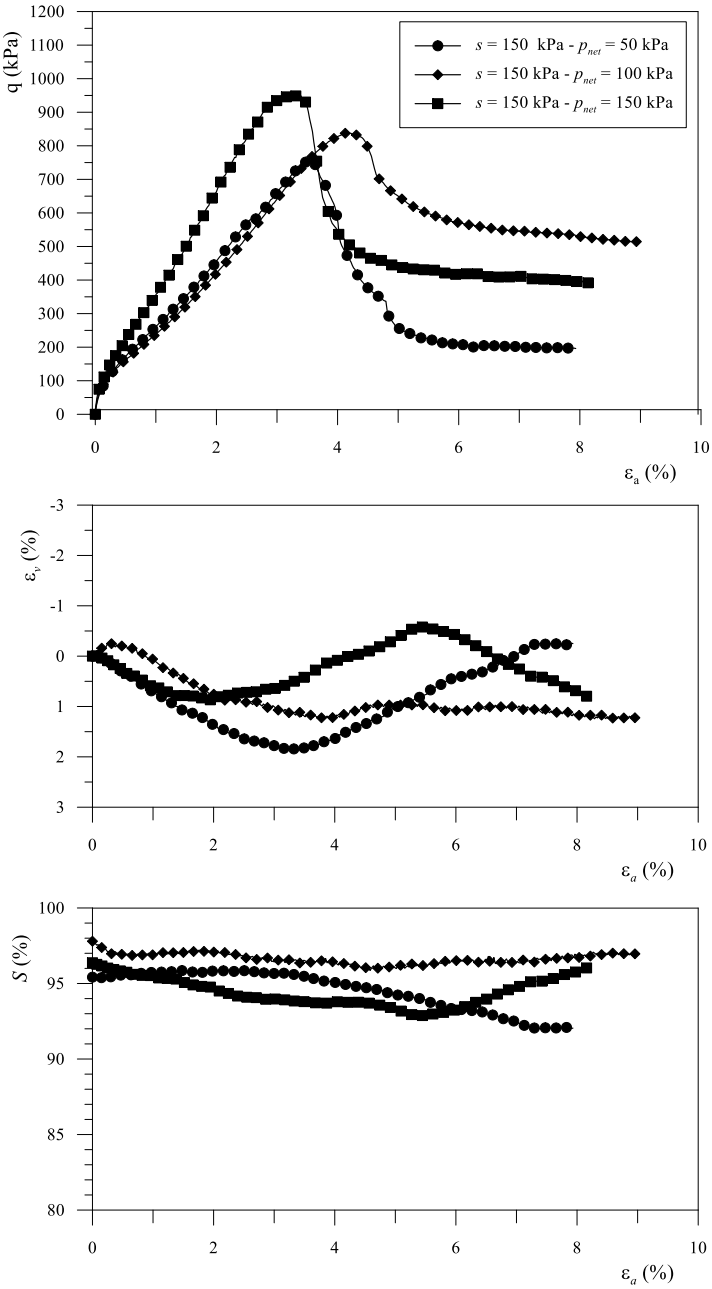

Figure 13 - Results of triaxial compression tests at *s* = 150 kPa.

Figure 14 - Specimen at the end of test.

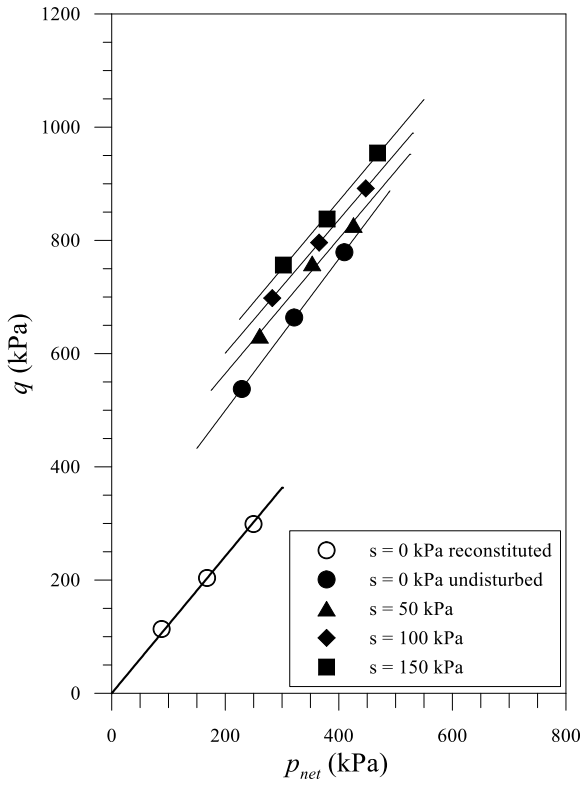

Figure 15 - Failure envelopes.

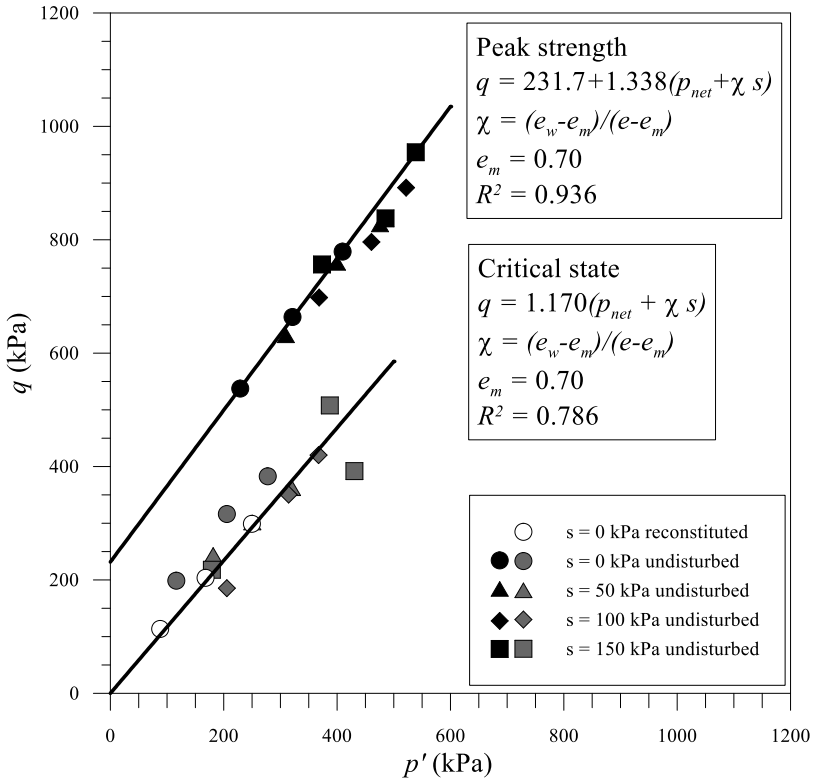
Peak strength
q = 231.7+1.338(p_{net}+χ s)
χ = (e_w-e_m)/(e-e_m)
e_m = 0.70
R^2 = 0.936
Critical state
q = 1.170(p_{net} + χ s)
χ = (e_w-e_m)/(e-e_m)
e_m = 0.70
R^2 = 0.786
s = 0 kPa reconstituted
s = 0 kPa undisturbed
s = 50 kPa undisturbed
s = 100 kPa undisturbed
s = 150 kPa undisturbed
q (kPa)
p' (kPa)
0
200
400
600
800
1000
1200

Figure 16 - Strength envelopes in terms of effective stress (grey points represent condition at critical state).